Femtosecond surface plasmon interferometry

Vasily V. Temnov[1], Keith Nelson[1], Gaspar Armelles[2], Alfonso Cebollada[2], Tim Thomay[3], Alfred Leitenstorfer[3] and Rudolf Bratschitsch[3]

[1]*Department of Chemistry, Massachusetts Institute of Technology, Cambridge, Massachusetts 02139, USA*

[2]*Instituto de Microelectrónica de Madrid-IMM (CNM-CSIC), 28760 Tres Cantos, Madrid, Spain*

[3]*Department of Physics and Center for Applied Photonics, University of Konstanz, D-78457 Konstanz, Germany*

temnov@mit.edu

Abstract: We demonstrate femtosecond plasmonic interferometry with a novel geometry. The plasmonic microinterferometer consists of a tilted slit-groove pair. This arrangement allows for (i) interferometric measurements at a single wavelength with a single microinterferometer and (ii) unambiguous discrimination between changes in real and imaginary parts of the metal dielectric function. The performance is demonstrated by monitoring the sub-picosecond dynamics of hot electrons in gold.

OCIS codes: (240.6680) Surface plasmons; (240.6648) Surface dynamics, (320.7100) Ultrafast measurements

References and links

1. C. Genet and T. W. Ebbesen, "Light in tiny holes," Nature **445**, 39–46 (2007).
2. P. Mühlschlegel, H.-J. Eisler, O. J. F. Martin, B. Hecht, and D. W. Pohl, "Resonant Optical Antennas," Science **208**, 1607–1609 (2005).
3. P. J. Schuck, D. P. Fromm, A. Sundaramurthy, G. S. Kino, and W. E. Moerner, "Improving the Mismatch between Light and Nanoscale Objects with Gold Bowtie Nanoantennas," Phys. Rev. Lett. **94**, 017 402 (2005).
4. J. Merlein, M. Kahl, A. Zuschlag, A. Sell, A. Halm, J. Boneberg, P. Leiderer, A. Leitenstorfer, and R. Bratschitsch, "Nanomechanical control of an optical antenna," Nature Photonics **2**, 230–233 (2008).
5. L. Novotny, "Effective Wavelength Scaling for Optical Antennas," Phys. Rev. Lett. **98**, 266 802 (2007).
6. E. Kretschmann and H. Raether, "Radiative decay of nonradiative surface plasmons excited by light," Z. Naturforsch. A **23**, 2135–2136 (1968).
7. T. W. Ebbesen, H. J. Lezec, H. F. Ghaemi, T. Thio, and P. A. Wolff, "Extraordinary optical transmission through sub-wavelength hole arrays," Nature **391**, 667 (1998).
8. W. H. Weber and G. W. Ford, "Optical electric-field enhancement at a metal surface arising from surface-plasmon excitation," Opt. Lett. **6**, 122–124 (1981).
9. M. van Exter and A. Lagendijk, "Ultrashort surface-plasmon and phonon dynamics," Phys. Rev. Lett. **60**, 49–52 (1988).
10. R. H. M. Groeneveld, R. Sprik, and A. Lagendijk, "Ultrafast relaxation of electrons probed by surface plasmons at a thin silver film," Phys. Rev. Lett. **64**, 784–787 (1990).
11. J. Wang, J. Wu, and C. Guo, "Resolving dynamics of acoustic phonons by surface plasmons," Opt. Lett. **32**, 719–721 (2007).
12. S. Ogawa, H. Nagano, H. Petek, and A. P. Heberle, "Optical dephasing in Cu(111) measured by interferometric two-photon time-resolved photoemission," Phys. Rev. Lett. **78**, 1339–1342 (1997).

#107495 - $15.00 USD Received 12 Feb 2009; revised 6 Apr 2009; accepted 26 Apr 2009; published 4 May 2009

13. H. Petek, H. Nagano, and S. Ogawa, "Hole decoherence of d-bands in copper," Phys. Rev. Lett. **83**, 832–835 (1999).
14. A. Kubo, N. Pontius, and H. Petek, "Femtosecond Microscopy of Surface Plasmon Polariton Wave Packet Evolution at the Silver/Vacuum Interface," Nano. Lett. **7**, 470–475 (2007).
15. M. Tong, A. S. Kirakosyan, T. V. Shahbazyan, and Z. V. Vardeny, "Ultrafast Response of Surface Electromagnetic Waves in an Aluminum Film Perforated with Subwavelength Hole Arrays," Phys. Rev. Lett. **100**, 056 808 (2008).
16. V. Halte, A. Benabbas, and J. Y. Bigot, "Surface plasmon dynamics in arrays of subwavelength holes: the role of optical interband transitions," Opt. Express **16**, 11 611–11 617 (2008).
17. K. F. MacDonald, Z. L. Samson, M. I. Stockman, and N. I. Zheludev, "Ultrafast active plasmonics," Nature Photon. **3**, 55–58 (2008).
18. V. V. Temnov, K. Sokolowski-Tinten, P. Zhou, and D. von der Linde, "Ultrafast imaging interferometry at femtosecond laser-excited surfaces," J. Opt. Soc. Am. B **23**, 1954–1964 (2006).
19. V. V. Temnov, K. Sokolowski-Tinten, P. Zhou, A. El-Khamhawy, and D. von der Linde, "Multiphoton Ionization in Dielectrics: Comparison of Circular and Linear Polarization," Phys. Rev. Lett. **97**, 237 403 (2006).
20. G. Gay, O. Alloschery, B. V. de Lesegno, C. O'Dwyer, J. Weiner, and H. J. Lezec, "The response of nanostructured surfaces in the near field," Nature Phys. **2**, 262–267 (2006).
21. V. V. Temnov, U. Woggon, J. Dintinger, E. Devaux, and T. W. Ebbesen, "Surface plasmon interferometry: measuring group velocity of surface plasmons," Opt. Lett. **32**, 1235–1237 (2007).
22. D. Pacifici, H. J. Lezec, and H. A. Atwater, "All-optical modulation by plasmonic excitation of CdSe quantum dots," Nature Phot. **1**, 402–406 (2007).
23. Y. Fedutik, V. V. Temnov, O. Schöps, U. Woggon, and M. V. Artemyev, "Exciton-Plasmon-Photon Conversion in Plasmonic Nanostructures," Phys. Rev. Lett. **99**, 136 802 (2007).
24. J. Gomis-Bresco, S. Dommers, V. V. Temnov, U. Woggon, M. Laemmlin, D. Bimberg, E. Malic, M. Richter, E. Scholl, and A. Knorr, "Impact of Coulomb scattering on the ultrafast gain recovery in InGaAs quantum dots," Phys. Rev. Lett. **101**, 256 803 (2008).
25. H. F. Schouten, N. Kuzmin, G. Dubois, T. D. Visser, G. Gbur, P. F. A. Alkemade, H. Blok, G. W. 't Hooft, D. Lenstra, and E. R. Eliel, "Plasmon-Assisted Two-Slit Transmission: Young's Experiment Revisited," Phys. Rev. Lett. **94**, 053 901 (2005).
26. M. Takeda, H. Ina, and S. Kobayashi, "Fourier-transform method of fringe-pattern analysis for computer-based topography and interferometry," J. Opt. Soc. Am. B **72**, 156–160 (1982).
27. T. Kreis, *Handbook of Holographic Interferometry* (John Wiley & Sons, New York, 2004).
28. V. V. Temnov, K. Sokolowski-Tinten, P. Zhou, B. Rethfeld, V. E. Gruzdev, A. El-Khamhawy, and D. von der Linde, "Ionization mechanisms in dielectrics irradiated by femtosecond laser pulses," Proc. SPIE **5448**, 1119–1126 (2004).
29. R. H. M. Groeneveld, R. Sprik, and A. Lagendijk, "Effect of a nonthermal electron distribution on the electron-phonon energy relaxation process in noble metals," Phys. Rev. B **45**, 5079–5082 (1992).
30. N. Del Fatti, C. Voisin, M. Achermann, S. Tzortzakis, D. Christofilos, and F. Vallée, "Nonequilibrium electron dynamics in noble metals," Phys. Rev. B **61**, 16 956–16 966 (2000).
31. V. E. Gusev and O. B. Wright, "Ultrafast nonequilibrium dynamics of electrons in metals," Phys. Rev. B **57**, 2878–2888 (1998).
32. C. K. Sun, Vallée, L. H. Acioli, E. P. Ippen, and J. G. Fujimoto, "Femtosecond-tunable measurement of electron thermalization in gold," Phys. Rev. B **50**, 15 337–15 348 (1994).
33. M. Bonn, D. Denzler, S. Funk, M. Wolf, S. S. Wellershoff, and J. Hohlfeld, "Ultrafast electron dynamics at metal surfaces: Competition between electron-phonon coupling and hot-electron transport," Phys. Rev. B **61**, 1101–1105 (2000).
34. C. S. Moreira, A. M. N. Lima, H. Neff, and C. Thirstrup, "Temperature-dependent sensitivity of surface plasmon resonance sensors at the goldwater interface," Sens. Actuators B **134**, 854–862 (2008).
35. R. Bonifacio and H. Morawitz, "Cooperative Emission of an Excited Molecular Monolayer into Surface Plasmons," Phys. Rev. Lett. **36**, 1559–1562 (1976).
36. V. V. Temnov and U. Woggon, "Superradiance and Subradiance in an Inhomogeneously Broadened Ensemble of Two-Level Systems Coupled to a Low-Q Cavity," Phys. Rev. Lett. **95**, 243 602 (2005).
37. A. V. Akimov, A. Mukherjee, C. L. Yu, D. E. Chang, A. S. Zibrov, P. R. Hemmer, H. Park, and M. D. Lukin, "Generation of single optical plasmons in metallic nanowires coupled to quantum dots," Nature **450**, 402–406 (2007).
38. S. Palomba and L. Novotny, "Nonlinear excitation of surface plasmon polaritons by Four-Wave Mixing," Phys. Rev. Lett. **101**, 056 802 (2008).

1. Introduction

The excitation of surface plasmons in metals is often associated with strong enhancement of electric fields, which triggered the development of many sensing applications in physics, chem-

#107495 - $15.00 USD Received 12 Feb 2009; revised 6 Apr 2009; accepted 26 Apr 2009; published 4 May 2009

istry and biology [1]. This field enhancement is due to the antenna effect in plasmonic nanostructures [2, 3, 4, 5] or due to phase-matched surface plasmon generation in spatially extended plasmonic structures. The two most famous examples of phase-matched excitation of surface plasmons are the Kretschmann geometry with a thin metal film on a prism [6] and the periodic arrangement of sub-wavelength holes [7].

Intensity enhancement factors up to 300 achievable with surface plasmons excited in thin metal films in Kretschmann geometry [8] motivated pioneering applications in the field of ultrafast optical measurements [9, 10]. Femtosecond surface plasmon based pump-probe measurements were used to monitor the evolution of acoustic phonons in impulsively heated metal films [9, 11] and to resolve the dynamics of an electron gas weakly excited by femtosecond laser pulses [10]. Triggered by the recent developments in nanoplasmonics and time-resolved two-photon photoemission spectroscopy [12, 13], experiments with ultrafast surface plasmon pulses have been extended to nanostructured metallic surfaces. Very recently, these advances allowed for monitoring the dynamics of surface plasmon pulses in silver gratings with unprecedented temporal and spatial resolution [14] and provided a better understanding of the mechanism for extraordinary transmission through arrays of sub-wavelength holes [15, 16]. A very recent degenerate ultrafast plasmonic experiment on a nanostructured metal surface revealed the role of laser-induced Kerr-type nonlinearity and transient grating incoupling for plasmon-assisted optical switching [17].

Here we report femtosecond time-resolved interferometry [18, 19] with a newly developed plasmonic microinterferometer [20, 21, 22]. It consists of a tilted slit-groove pair of sub-wavelength width, which enables interferometric measurements at a single optical wavelength with high spatial resolution. To demonstrate the capabilities of the technique we interferometrically probed the ultrafast hot carrier relaxation in gold with femtosecond surface plasmon pulses. These measurements allow for the unambiguous discrimination of small changes in the real and imaginary parts of the metal dielectric function. Our technique has the potential to extend time-resolved investigations of active plasmonic devices functionalized with nano-scale light emitters [22, 23] to the femtosecond time scale. These investigations are of crucial importance to explore capabilities for incorporation of ultra-wideband quantum dot based optical devices [24] in highly integrated plasmonic circuits.

2. Plasmonic microinterferometers

Figure 1(a) shows a scanning electron microscope (SEM) image of the plasmonic microinterferometer, which consists of a slit-groove pair milled into a 200 nm gold film with a 30 kV Ga^+ focussed ion beam. The 200 nm gold film was grown by magnetron sputtering on a 2 nm thin chromium buffer layer on a glass substrate. The length of both the slit and the groove is 50 μm. The slit has a width of 100 nm and extends through the gold layer. The groove is 100 nm deep and 200 nm wide. A series of similar structures was fabricated, with the slit-groove tilt angle varied between 3° and 15° and the slit-groove distance between 0 and 50 μm. If the whole area of the microinterferometer is homogeneously illuminated with light, surface plasmons generated at the groove propagate toward the slit and interfere with the directly transmitted light. In contrast to the parallel slit-groove arrangements used in previous studies [20, 21, 22], a small tilt angle between the slit and the groove allows for interferometric measurements at a single wavelength with a single microinterferometer.

A transmission image of a slit-groove microinterferometer illuminated by a collimated p-polarized laser beam (incidence angle 10 degrees away from normal, beam waist ~ 40 μm FWHM, $\lambda = 800$ nm, pulse duration $\sim$200 fs) is shown in Fig. 1(b). A bright periodic intensity modulation of light transmitted through the silt is clearly visible. Since the strongest interference maxima are saturated in the video camera image of Fig. 1(b) the much weaker

#107495 - $15.00 USD Received 12 Feb 2009; revised 6 Apr 2009; accepted 26 Apr 2009; published 4 May 2009

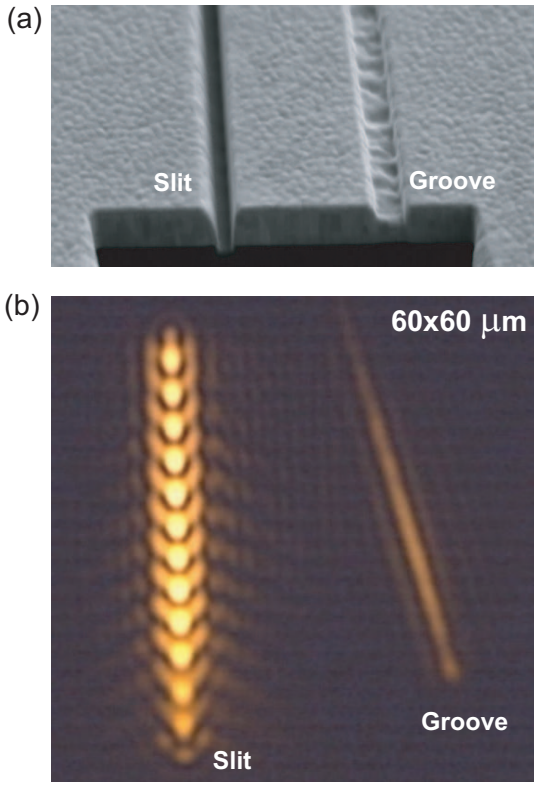

Fig. 1. Plasmonic microinterferometer with a tilted slit-groove pair. (a) SEM image showing a typical depth profile of the slit-groove structure (slit-groove distance 1 μm, slit-groove tilt angle $\Theta = 3^\circ$, slit width 100 nm, groove width 200 nm, groove depth 100 nm) milled into a 200 nm thick gold film on glass by a focussed ion beam. (b) Optical transmission of a homogeneously illuminated microinterferometer with a minimum slit-groove spacing of $d_0 = 20$ μm and slit-groove tilt angle $\Theta = 15^\circ$. The periodic modulation of light intensity transmitted through the slit is due to interference with surface plasmons launched by the groove (see text for details).

symmetrical diffraction wings on both sides of the slit are clearly visible. The peculiar orientation of diffraction wings is correlated with the orientation of the groove and depicts the role of surface plasmons generated by the groove. A small amount of residual transmission through the sub-wavelength groove shows its position and orientation. Due to the tilt angle Θ, the distance $d(x) = d_0 + x\sin(\Theta)$ traversed by surface plasmons on the way from the groove to the slit varies linearly along the slit axis x, resulting in a sinusoidal interference pattern:

$$I(x) = E_1(x)^2 + E_2(x)^2 + 2E_1(x)E_2(x)\cos(\Phi(x))\,, \tag{1}$$

where $E_1(x)$ is the amplitude of light directly transmitted through the slit and the plasmonic contribution is given by

$$\begin{aligned} E_2(x) &\sim \exp(-k_{\mathrm{sp}}^{''} d(x))\,, \\ \Phi(x) &= k_{\mathrm{sp}}^{'} d(x) + \phi_0\,. \end{aligned} \tag{2}$$

The amplitude of the surface plasmon at the position of the slit $E_2(x)$ is attenuated by a factor of $\exp(-k_{\mathrm{sp}}^{''} d(x))$ due to the finite propagation distance $L_{\mathrm{sp}} = 1/2k_{\mathrm{sp}}^{''}$ of the surface plasmons

#107495 - $15.00 USD Received 12 Feb 2009; revised 6 Apr 2009; accepted 26 Apr 2009; published 4 May 2009

($L_{sp} = 45\ \mu$m at 800 nm for a gold-air interface [25]). The total phase shift $\Phi(x)$ is the sum of the plasmonic phase $k'_{sp}d(x)$ acquired through propagation and a constant unknown phase ϕ_0 due to differences in propagation length in air and to in- and out-coupling of surface plasmons at the groove and at the slit, respectively. The key idea behind surface plasmon interferometry is to accurately measure the changes of the complex surface plasmon wave vector $k_{sp} = k'_{sp} + ik''_{sp}$ upon external perturbation.

3. Femtosecond plasmonic interferometry

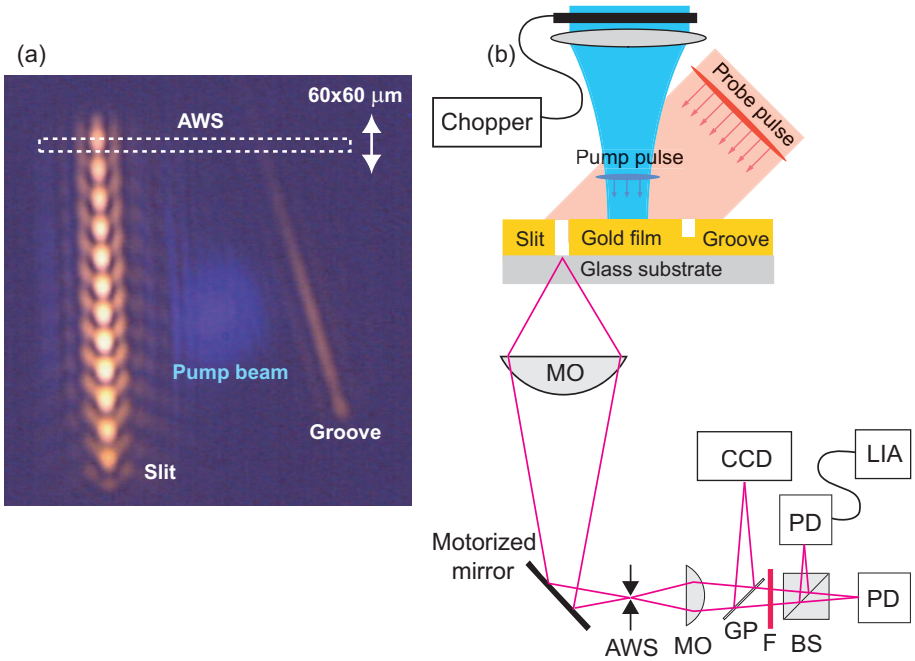

Fig. 2. Overview of the femtosecond plasmon interferometry technique. (a) Pump-probe excitation geometry of the plasmonic slit-groove microinterferometer: the probe spot illuminates the whole area of the microinterferometer. The pump beam (blue) is focussed to a 10 μm spot between the slit and the groove. (b) Experimental geometry for scanning pump-probe measurements. (PD - photodiode, MO - microscope objective, BS- beam splitter, AWS - adjustable width slit, GP - glass plate, F - color absorption filter, LIA - lock-in amplifier).

The analysis of the plasmonic interference pattern in the previous section is valid for pulsed excitation sources as long as (i) the time of flight of an ultrashort surface plasmon pulse traveling between the groove and the slit is shorter than the pulse duration so that both components interfere with each other at the slit and (ii) the temporal structure of the ultrashort surface plasmon pulse is not significantly influenced by dispersion. In our case both conditions are fulfilled: (i) the slit-groove distance in the range of $\sim 30\ \mu$m results in group delays on the order of 100 fs, which is less than the 200 fs pulse duration of our Ti:sapphire femtosecond laser source, and (ii) the group velocity dispersion for our surface plasmon pulses at 800 nm is small. Thus the transmission image of the microinterferometer shown in Fig. 1(b) clearly reveals alternative constructive and destructive superposition of field components arriving at the slit from free space and from the groove.

#107495 - $15.00 USD Received 12 Feb 2009; revised 6 Apr 2009; accepted 26 Apr 2009; published 4 May 2009

We apply a femtosecond laser pulse to excite the gold surface between the slit and the groove. A transient perturbation of the metal dielectric function is created and probed with time-delayed surface plasmon pulses. To do this the output of an amplified Ti:sapphire laser ($\lambda = 800$ nm, repetition rate 250 kHz, pulse duration 200 fs, average power 200 mW) is split into pump and probe arms. Pump pulses ($\lambda = 400$ nm, pulse duration 150 fs, average power 160 μW) are generated by frequency doubling in a 300 μm-thick BBO crystal. The pump beam is mechanically chopped at 1.5 kHz and focussed under normal incidence to a 10 μm symmetrical spot on the sample between the slit and the groove. The residual transmission of the pump beam through the gold film can be seen in Fig. 2(a). The probe beam (50 mW average power) is focussed at 10 degrees from normal incidence into a significantly larger spot of 40 μm to illuminate the entire area of the microinterferometer. Whereas nearly 98% of incident probe light is reflected from the gold surface, 75% of the pump energy is absorbed. We achieved the best contrast in the plasmonic interference pattern by centering the probe beam on the groove in order to increase the relative amplitude of the surface plasmon pulses as compared to the amplitude of directly transmitted light. A motorized delay stage in the pump arm was used to vary the time delay between pump and probe pulses in the range of 0 to 1 ns with a minimum step size of 2 fs. The back surface of the gold film (object plane) was imaged after reflection from a mirror positioned on a motorized mirror mount to an intermediate image plane by a microscope objective (10x magnification, NA = 0.28), where a high-precision adjustable width slit (AWS) is placed. By closing the slit to about 20 μm only a small part of the image can be selected (as shown by the dashed contour in Fig. 2(a)) and sent to a detection unit consisting of a silicon CCD camera and a pair of silicon photodiodes. One of the reflection angles controlled by the motorized mirror can be varied so that the microinterferometer image is shifted in the vertical direction of Fig. 2a, along the slit direction. The small horizontal band of the microinterferometer image that is transmitted through the adjustable width slit (AWS) to the detection system is thereby varied. The DC signal from one photodiode is used to record the spatially varying intensity of the plasmonic interference pattern. The modulated part of the current from the other photodiode is spectrally filtered, amplified by a low-noise current preamplifier, and measured by a lock-in amplifier locked to the frequency of the mechanical chopper. A color absorption filter is used to block the residual transmission of the pump beam modulated at the same frequency. A calibration of the amplitude of this modulated pump-probe signal as compared to the interferogram intensity is performed in a reference measurement: when the pump beam is blocked and the probe beam is chopped at the same frequency both photodiodes record the plasmonic interferogram intensity with very different amplitudes.

Scanning the optical delay line and the motorized mirror angle allows us to record the plasmonic interference pattern along the slit direction and its pump-induced changes as a function of pump-probe delay (Fig. 3). The upper panel shows the intensity distribution $I(x,\tau)$ of the plasmonic interference pattern along the slit direction measured during the scan. Since the pump-induced changes are small, the periodic interference pattern in Fig. 3(a) does not exhibit a noticeable dependence on the pump-probe delay time. In comparison Fig. 3(b) depicts the amplitude of the modulated pump-probe signal $I_{pp}(x,\tau)$ acquired by the lock-in amplifier. A prominent positive signal is observed at zero time delay followed by transient dynamics on a picosecond time scale.

To verify that the observed pump-probe signal is dominated by the plasmonic contribution we performed additional test measurements under the same pump conditions but using (i) s-polarized probe pulses which do not generate surface plasmons [25] and (ii) structures that included the sub-wavelength slit but not the groove. No noticeable pump-probe signal was observed in these two control measurements.

#107495 - $15.00 USD Received 12 Feb 2009; revised 6 Apr 2009; accepted 26 Apr 2009; published 4 May 2009

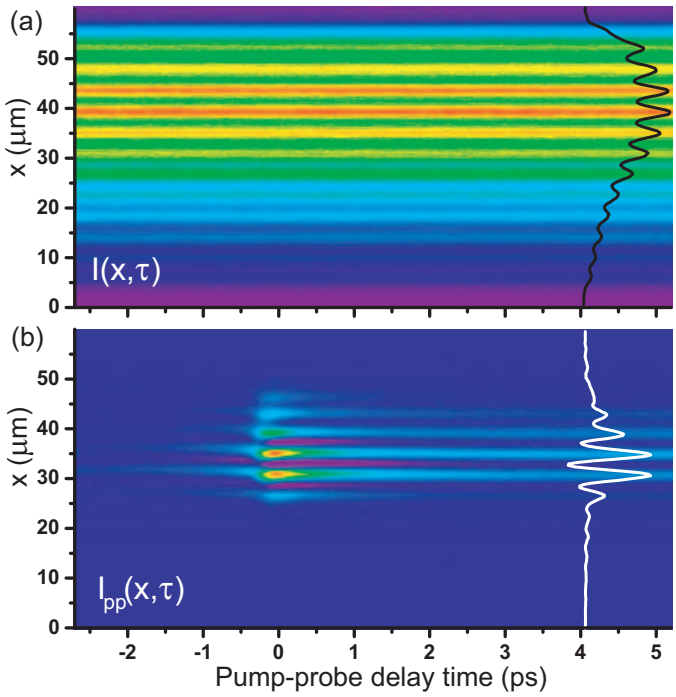

Fig. 3. Plasmonic interferograms for slit-groove microinterferometer with $d_0 = 20\ \mu$m and $\Theta = 15^\circ$. (a) Plasmonic interference pattern $I(x,\tau)$ (b) Plasmonic pump-probe interferogram $I_{\rm pp}(x,\tau)$.

4. Analysis of plasmonic pump-probe interferograms

We now discuss the physical origin of the observed pump-probe signal. Intense photo-excitation of gold is known to modify both the real and imaginary parts of its linear dielectric susceptibility $\varepsilon = \varepsilon^{'} + i\varepsilon^{''}$. Therefore both the real and imaginary parts of complex surface plasmon wave vector

$$k_{\rm sp} = k_0\sqrt{\frac{\varepsilon}{1+\varepsilon}} \tag{3}$$

change as well. Here $k_0 = \omega/c$ denotes the wave vector magnitude of the probe light in vacuum. The pump-probe signal I_{pp} is then obtained by taking a derivative of $I(x)$ with respect to $\delta k_{\rm sp} = \delta k^{'}_{\rm sp} + i\delta k^{''}_{\rm sp}$:

$$I_{pp} = -2E_1E_2(dk^{''}_{\rm sp}\cos\Phi + dk^{'}_{\rm sp}\sin\Phi)L_{int}\,. \tag{4}$$

The effective interaction length L_{int} is of the order of the diameter of the spot excited by the pump beam, which in our case is $\sim 10\mu$m. When deriving Eq. (4) we have neglected possible changes of $E_2(x)^2$ in Eq. (1), which provide a featureless background proportional to the spatial pump intensity distribution. The pump-probe interferogram (4) consists of two oscillating terms proportional to $\cos\Phi$ and $\sin\Phi$ that arise from pump-induced changes in surface plasmon amplitude and phase, respectively. The general expression (4) can be simplified. Since for the probe wavelength of 800 nm, $|\varepsilon| \gg 1$ and $|\varepsilon^{'}| \gg \varepsilon^{''}$, the dispersion relation for surface plasmons can be approximated by

$$k_{\rm sp} \simeq k_0\left(1 - \frac{1}{2\varepsilon}\right). \tag{5}$$

#107495 - $15.00 USD Received 12 Feb 2009; revised 6 Apr 2009; accepted 26 Apr 2009; published 4 May 2009

The change of the real and imaginary parts of complex surface plasmon wave vector

$$dk_{\mathrm{sp}}^{'} \simeq \frac{k_0}{2|\varepsilon|^2} d\varepsilon^{'}, dk_{\mathrm{sp}}^{''} \simeq \frac{k_0}{2|\varepsilon|^2} d\varepsilon^{''} \tag{6}$$

appear to be proportional to the change of real and imaginary parts, respectively, of the dielectric function of the metal $\delta\varepsilon = \delta\varepsilon^{'} + i\delta\varepsilon^{''}$. The simplified expression for the pump-probe signal I_{pp}, adopted to our experimental conditions,

$$I_{pp} = -E_1 E_2 \frac{k_0 L_{int}}{|\varepsilon|^2} (d\varepsilon^{''} \cos\Phi + d\varepsilon^{'} \sin\Phi), \tag{7}$$

provides direct access to the dynamics of the dielectric response of the metal. Considering the two-dimensional maps in Fig. 3 as a collection of one-dimensional interferograms acquired at different pump-probe delay times, we have processed these one-dimensional interferograms using a standard Fourier-based algorithm [26]. Both the pump-probe $I_{pp}(x)$ and reference intensity interferograms $I(x)$ were processed by the same algorithm. The analysis of the reference interferogram $I(x)$ provides the amplitude factor $E_1(x)E_2(x)$ and the reference phase $\Phi(x)$ in Eq. (7), which allows for the reconstruction of the desired quadrature components $d\varepsilon^{'}$ and $d\varepsilon^{''}$ from the analysis of $I_{pp}(x)$. This processing is applied for interferograms with different pump-probe delay times to generate two-dimensional maps $d\varepsilon^{'}(x,\tau)$ and $d\varepsilon^{''}(x,\tau)$, which are presented in Fig. 4.

5. Results and discussion

There are several approaches to extraction of quantitative information from the results in Fig. 4. The most rigorous one would rely on a detailed analysis of the spatial profiles for every pump-probe delay time, based on the Abel transformation [27] exploiting the cylindrical symmetry of our excitation pump spot. This approach could be useful when the optical response depends strongly on pump intensity. Since the recorded time-dependent signals (cross-sections in Fig. 4 taken at different positions x) all are similar, we restrict ourselves to the analysis of one time-dependent trace at the maximum signal level (x$\sim$ 33 μm). The results are shown in Fig. 5.

We observe similar signals for both real and imaginary parts $d\varepsilon^{'}(\tau)$ and $d\varepsilon^{''}(\tau)$. The dynamics close to zero time delay are complicated, with some positive $d\varepsilon^{'}(\tau)$ and negative $d\varepsilon^{''}(\tau)$ signals at negative delay times. Since it is generally difficult to analyze such cross-phase modulation effects even in simple geometries [28], we will focus on the dynamics at positive time delays. The real and imaginary parts $d\varepsilon^{'}(\tau)$ and $d\varepsilon^{''}(\tau)$ have approximately the same maximum amplitude and they both decay monotonously on a time scale of hundreds of femtoseconds, reaching a plateau at 5 ps delay, followed by slower dynamics on a time scale of several tens of picoseconds (not shown). A detailed study of coherent acoustic responses is beyond the scope of this paper, but we mention that at longer pump-probe delay times of the order of tens of picoseconds, the signatures of acoustic oscillations in the gold film appear, in agreement with previous experimental observations [9, 11].

Inspection of the curves on a logarithmic scale (see subplot in Fig. 5, with subtracted background values at 5 ps) reveals that the real part of the dielectric function $d\varepsilon^{'}(\tau)$ decays exponentially with a single time constant of 900 fs. This decay time is in excellent agreement with the electron-phonon relaxation time of laser-heated electrons in gold [29, 30, 31]. The dynamics of the imaginary part $d\varepsilon^{''}(\tau)$ shows a pronounced bi-exponential decay with a fast component of 500 fs followed by a longer decay of 900 fs. The fast dynamics in $d\varepsilon^{''}(\tau)$ are in agreement with previous time-resolved measurements of non-equilibrium electron thermalization and optical

#107495 - $15.00 USD Received 12 Feb 2009; revised 6 Apr 2009; accepted 26 Apr 2009; published 4 May 2009

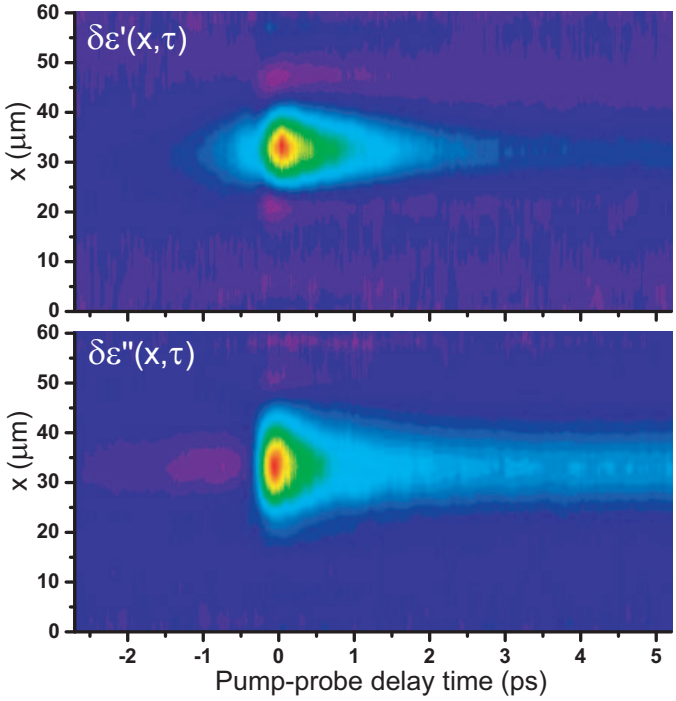

Fig. 4. Spatial and temporal dependence of the recorded pump-induced changes of real and imaginary parts of the complex dielectric function of gold, $d\varepsilon^{'}(x,\tau)$ and $d\varepsilon^{''}(x,\tau)$.

non-linearities in Au [30, 32]. We believe that the observed decay of 500 fs is due to electron-electron thermalization [31, 32] and a possible transient nonlinearity due to the creation of the d-band holes [12, 13] (our laser pulses are of 200 fs duration).

A few picoseconds after laser excitation a thermal equilibrium between initially hot electrons and the cold lattice is established. The observed signal at that time delay can be interpreted in terms of a temperature-dependent change of metal dielectric function [10, 33]. Owing to the small penetration depth of the surface plasmon in the metal we are probing the surface temperature in the vertical direction within the skin depth of $\sim$ 13 nm (at 800 nm). Using the calculated values for the derivatives $d\varepsilon^{'}/dT = 1.8\times10^{-3}$ K^{-1} and $d\varepsilon^{''}/dT = 4.5\times10^{-3}$ K^{-1} [34], we obtain good agreement with the values of $d\varepsilon^{'}(\tau = 5\text{ ps}) = 0.04$ and $d\varepsilon^{'}(\tau = 5\text{ ps}) = 0.09$ assuming an increase in surface temperature of 20 K, which is a reasonable result.

It has been previously shown in a three-pulse experiment [33] that the temperature distribution inside the fs-excited gold film remains spatially inhomogeneous for tens of picoseconds after excitation. The assumption of a homogeneously heated gold film provides a lower bound for the surface temperature of 10 K, derived from conservation of the absorbed laser energy. Therefore the experimentally estimated temperature of 20 K suggests that five picoseconds after laser excitation the temperature distribution inside the gold film is still spatially inhomogeneous, in agreement with [33].

6. Conclusions and Outlook

We have presented a new experimental technique of time-resolved imaging interferometry with ultrashort surface plasmon pulses in a tilted slit-groove plasmonic microinterferometer. The method allows pump-induced changes in surface plasmon behavior to be monitored and related

#107495 - $15.00 USD Received 12 Feb 2009; revised 6 Apr 2009; accepted 26 Apr 2009; published 4 May 2009

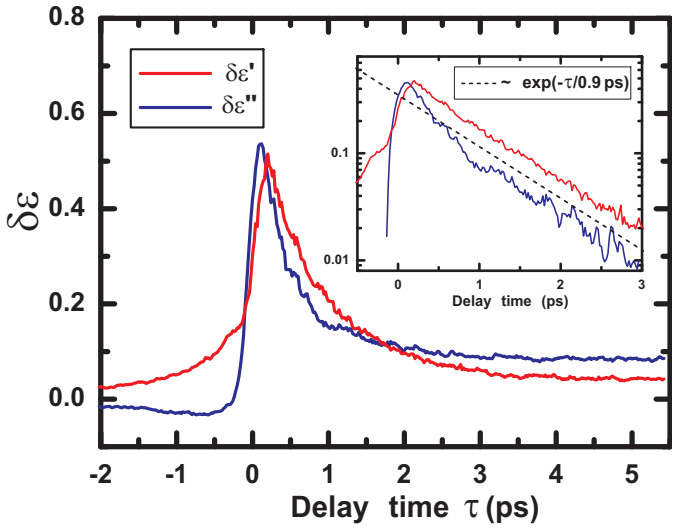

Fig. 5. Transient pump-induced changes of real and imaginary parts of the complex dielectric function of gold, $d\varepsilon^{'}(\tau)$ and $d\varepsilon^{''}(\tau)$.

with high accuracy and spatial resolution to distinct pump-induced changes in the real and imaginary parts of the metal dielectric function. The approach opens the door for simultaneous manipulation and phase-sensitive observation of ultrashort surface plasmons in two dimensions. Functionalization of two-dimensional microinterferometers with nonlinear optical materials offers a variety of applications in the emerging fields of quantum optics [23, 35, 36, 37] and nonlinear optics with surface plasmons [17, 38].

Acknowledgements

The financial support of Deutsche Forschungsgemeinschaft (TE770/1), the National Science Foundation (CHE-050714), the EU Network of Excellence "PhOREMOST", NMP3-SL-2008-214107-Nanomagma, FUNCOAT CONSOLIDER INGENIO 2010 CSD2008-00023, MAGPLAS MAT2008-06765-C02-01/NAN, NANOMAGNETCMS-0505/MAT/0194 and MICROSERES S-0505/TIC/0191 is acknowledged. We are grateful to Christoph Klieber and Christopher Werley for technical assistance at MIT.

#107495 - $15.00 USD Received 12 Feb 2009; revised 6 Apr 2009; accepted 26 Apr 2009; published 4 May 2009